Large-Area Free-Standing Ultrathin Single-Crystal Silicon as Processable Materials

Shuang Wang,[†] Benjamin D. Weil,[‡] Yanbin Li,[‡] Ken Xingze Wang,[†] Erik Garnett,[‡] Shanhui Fan,[†] and Yi Cui*[,‡,§]

[†]Department of Electrical Engineering, Stanford University, Stanford, California 94305, United States

[‡]Department of Materials Science and Engineering, Stanford University, Stanford, California 94305, United States

[§]Stanford Institute for Materials and Energy Sciences, SLAC National Accelerator Laboratory, 2575 Sand Hill Road, Menlo Park, California 94025, United States

S *Supporting Information*

ABSTRACT: Silicon has been driving the great success of semiconductor industry, and emerging forms of silicon have generated new opportunities in electronics, biotechnology, and energy applications. Here we demonstrate large-area free-standing ultrathin single-crystalline Si at the wafer scale as new Si materials with processability. We fabricated them by KOH etching of the Si wafer and show their uniform thickness from 10 to sub-2 μm. These ultrathin Si exhibits excellent mechanical flexibility and bendability more than those with 20−30 μm thickness in previous study. Unexpectedly, these ultrathin Si materials can be cut with scissors like a piece of paper, and they are robust during various regular fabrication processings including tweezer handling, spin coating, patterning, doping, wet and dry etching, annealing, and metal deposition. We demonstrate the fabrication of planar and double-sided nanocone solar cells and highlight that the processability on both sides of surface together with the interesting property of these free-standing ultrathin Si materials opens up exciting opportunities to generate novel functional devices different from the existing approaches.

KEYWORDS: *Ultrathin single-crystal silicon, flexibility, nanotexture, light trapping*
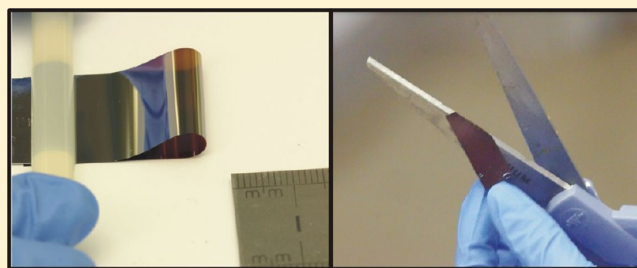
Silicon as one of the most important materials has been driving the great success of electronics, optoelectronics, and solar cell industries, where it is used in form of single- and multicrystalline wafers and amorphous and nanocrystalline film.[1−4] Recently new forms of Si have attracted great attention, such as bottom-up synthesized nanowires,[5,6] nanotubes,[7] nanocrystals,[8] microwires[9] and top-down etched ribbons,[10,11] wires,[12,13] porous Si,[14] suspended thin membrane in silicon-on-insulator[15] and thin film by stress-induced mechanically peeling.[16,17] These emerging Si materials have enabled new opportunities in electronics,[17] bioelectronics,[18,19] solar energy conversion,[12,20] thermoelectrics,[21] and batteries.[22,23] Here we demonstrate large-area free-standing ultrathin single-crystalline Si at the wafer scale as new Si materials with processability. We fabricated them by KOH etching of the Si wafer and show their uniform thickness from 10 to sub-2 μm. These ultrathin Si exhibits excellent mechanical flexibility and bendability more than those with 20−30 μm thickness in a previous study.[24] Unexpectedly, these ultrathin Si materials can be cut with scissors like a piece of paper, and they are robust during various regular fabrication processings including tweezer handling, spin coating, patterning, doping, wet and dry etching, annealing, and metal deposition. We demonstrate the fabrication of planar and double-sided nanocone solar cells and highlight that the

processability on the surfaces of both sides together with the interesting property of these free-standing ultrathin Si materials opens up exciting opportunities to generate novel functional devices different from the existing approaches.

We fabricated thin single-crystal Si by KOH solution etching of Si wafers or pieces of Si wafers at control temperature of 90 °C (see Methods for details). At 90 °C, the etching rate is about 80 μm/h. It is remarkable that the whole wafer with about 350 μm thickness can be etched uniformly down to few micrometers except at the edge of wafer where a ring fixture blocks the etching solution. This etching technique enables us to carry out proof-of-principles exploration of ultrathin silicon films as we report here. The unique and exciting properties of ultrathin silicon film as demonstrated here should provide further motivation for the developments of fabrication techniques that create ultrathin film while minimizing material usage.

Figure 1a illustrates the optical image of the resulted thin Si films with underneath white light illumination and the scanning electron microscope (SEM) images of the cross sections. The Si thicknesses from left to right are 10.7 μm, 6.4 μm, 5.4 μm,
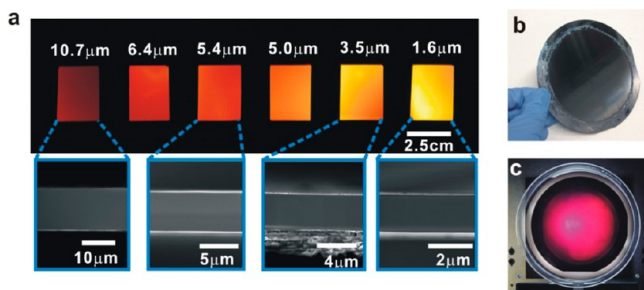
Figure 1. Color spectrum of the ultrathin Si films. (a) Si films with different thicknesses illuminated by white light from the backside. The inserted images are the SEM images of the cross sections of the 10.7 μm, 5.4 μm, 3.5 μm, and 1.6 μm thick films. (b) Optical image of a 4-in. wafer-size ultrathin Si films (c) The 4-in. wafer size ultrathin Si film illuminated by the white light source of a solar simulator from the backside.

5.0 μm, 3.5 μm, and 1.6 μm, respectively. As the film becomes thinner and thinner, its color gradually changes from dark red to bright yellow, due to insufficient light absorption. The absorption depth of certain wavelength is defined as the distance into the material at which the light drops to about 36% of its original intensity. When the Si film is etched down to 1.6 μm thick, where the film thickness equals to the light absorption depth of light with wavelength of 552 nm, the yellow light (with wavelength of about 570 nm) cannot be sufficiently absorbed by a single path through the film, thus mostly transmitting through it, resulting a bright yellow color of the 1.6 μm film shown in Figure 1a. For the 10.7 μm thick film, where the film thickness equals to light absorption depth of 789 nm light, yellow light is absorbed, whereas the red light (with wavelength of about 600 nm) partially transmits through it, leaving a dark red color in Figure 1a. The color of the other films ranging from red to orange corresponds to the absorption spectrum cutoffs by different thicknesses. Table 1 summarizes the absorption depth of different wavelengths for Si, which matches well with the thin Si color shown in Figure 1a.

Table 1. Light Absorption Depth in Si

| absorption depth (μm)	10.7	6.4	5.4	5	3.5	1.6
wavelength (nm)	790	728	704	693	648	552

We have successfully demonstrated ultrathin film etching from up to 4-in. Si wafers, and we believe that such an etching method can be used for an even larger size Si. Figure 1b shows an example of 4-in. diameter free-standing thin Si film, whose thickness is around 11 μm. It exhibits red color on the white light source of a solar simulator, as shown in Figure 1c. The edge ring of this sample is thicker than the inner area, because a Teflon mask is used in the etching.

The free-standing ultrathin single-crystalline Si films with thickness less than 10 μm exhibit excellent mechanical flexibility. Figure 2a shows a Si film with a thickness of 3 μm wrapped around a rod with diameter of 7 mm, and Figure 2b shows two images of the beginning and the end of the folding process of a thin film. The Si film is folded with a bending radius of 1 mm at the end. While in the past, mechanical flexibility has been demonstrated for Si wafer with thickness of 20−50 μm[24] and for Si nano/microstructures with a thickness of less than 1 μm,[10,25] the study here highlights the extreme

mechanical flexibility on large-area Si films of several micrometers thick.

Furthermore, the films are mechanically robust enough to be handled without advanced support in device fabrication processes. They can be directly manipulated by hand and tweezers and be processed in solutions (see Supporting Information, Video 1). It is remarkable that the thin Si films can also be cut using scissors along any directions without breaking them, which is similar to cutting papers (Figure 2c and Supporting Information, Video 2). Figure 2d illustrates the ultrathin Si films of square, parallelogram, triangular, and heptagon shapes cut by scissors. The cutting is smooth and straight when it is along the certain crystalline directions, such as those of the square shape, whereas, when it is off the crystalline directions, it results in a jagged edge, such as sides A and B of the parallelogram, and sides C and D of the triangle. The magnified optical microscope images of smooth and jagged edges are shown in Figure 2e. It can be seen that the cracks have favorable propagation directions which are along the ⟨110⟩ family of crystallographic directions, cutting with a direction that deviates from these directions results in a jagged edge. We believe that the capability of scissor cutting is due to the ultrasmall thinness of Si films here, which prevent the propagation of the mechanical cracks to the whole area of Si. Besides the handling and cutting, we have also applied a variety of processing methods to these thin Si without breaking them. These include patterning by both dry etching and wet etching processes to introduce surfaces nanostructures for light trapping, spin-coating, doping, annealing, and metal deposition, opening up the opportunity for fabricating electronic and optoelectronic devices, which is illustrated in detail in the following parts.

We demonstrate the processability of these ultrathin Si films without supporting substrates by using an example of solar cell fabrication. Single crystalline Si solar cell dominates the PV market. There is a significant recent interest in designing ultrathin crystalline Si solar cells with active layer thickness of a few micrometers, which requires considerable improvements in light absorption. Light trapping through nanoscale texturing is one promising approach to enhance light absorption.[26−28] It is reported that through optimized design of the geometries of the surface nanotextures, photocurrent generated by ultrathin absorbers is able to reach the Yablonovitch limit.[29] Here, we experimentally demonstrated a large light absorption enhancement by the double-sided surface nanotexture design on free-standing ultrathin Si films. By combining Langmuir−Blodgett (LB) assembly with reactive ion etching (RIE),[30] we first introduce a nanocone array on one side of the ultrathin Si film. Then by repeating the same fabrication procedure, another nanocone array is patterned on the other side of the film. Figure 3a−e illustrates the SEM images of the double-sided nanotextured Si films. The front-side nanocone array is designed for broad-band antireflection over the entire usable solar spectrum. It has a periodicity of 450 nm and height of about 1.5 μm. The back-side pattern is designed for light trapping roughly in the 800−1100 nm wavelength range. It has a periodicity of 1000 nm and height of about 270 nm. We study the light trapping effect by comparing the light absorption of the ultrathin Si films without surface patterning (Figure 3d), with front-side patterning (Figure 3e), and with double-sided patterning (Figure 3f). Figure 3d illustrates the absorption spectrum for Si films without surface patterning, with thicknesses of 3 μm, 7 μm, 20 μm, and 48 μm. It can be
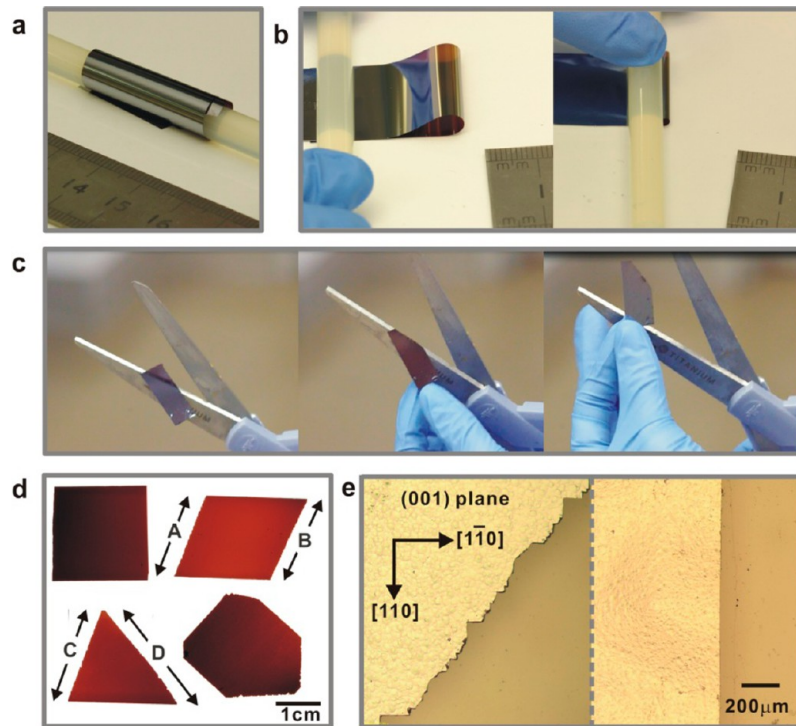
Figure 2. Flexible ultrathin Si films and Si films with various shapes cut by shears . (a) A 3 μm thick Si film was wrapped around a plastic rod with diameter of 7 mm. (b) The Si film was folded and then pressed by the plastic rod. The minimum folding radius is around 1 mm. (c) Optical scope image of the cutting edge of the thin Si film when cut not along crystalline directions. (d) Scissor-cut Si films with square, parallelogram, triangular, and heptagon shapes. (e) Magnified optical images of film edges by scissor cutting along (left) and off (right) Si crystalline direction.
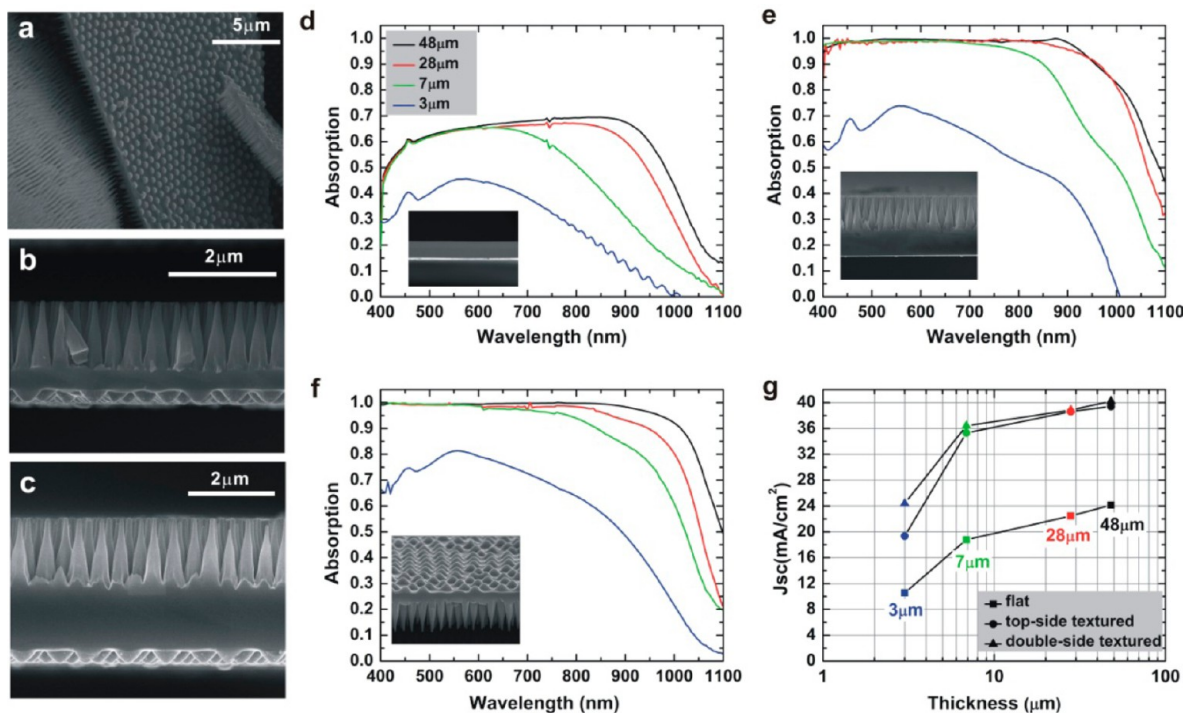
Figure 3. Enhancement of light absorption and photon generated current by the double-sided nanopatterning. (a) SEM images of three pieces double-sided patterned films, which shows both the front-side nanocone array and the back-side nanodome array in a large area. (b and c) SEM images showing the cross sections of two different double-sided patterned films. (d−f) Absorption spectra of Si films with thicknesses of 3 μm, 7 μm, 28 μm, and 48 μm without surface textures, with front-side nanotexture, and with double-sided nanotextures, respectively. (g) Enhancements of the photon generated currents in the 3 μm, 7 μm, 28 μm, and 48 μm thick flat Si films by the front-side nanotexture, and by the double-sided nanotextures. The data points in square shapes are for flat films, those in circular shapes are for the front-side patterned films, and the triangular shape data points are for the double-sided patterned films.
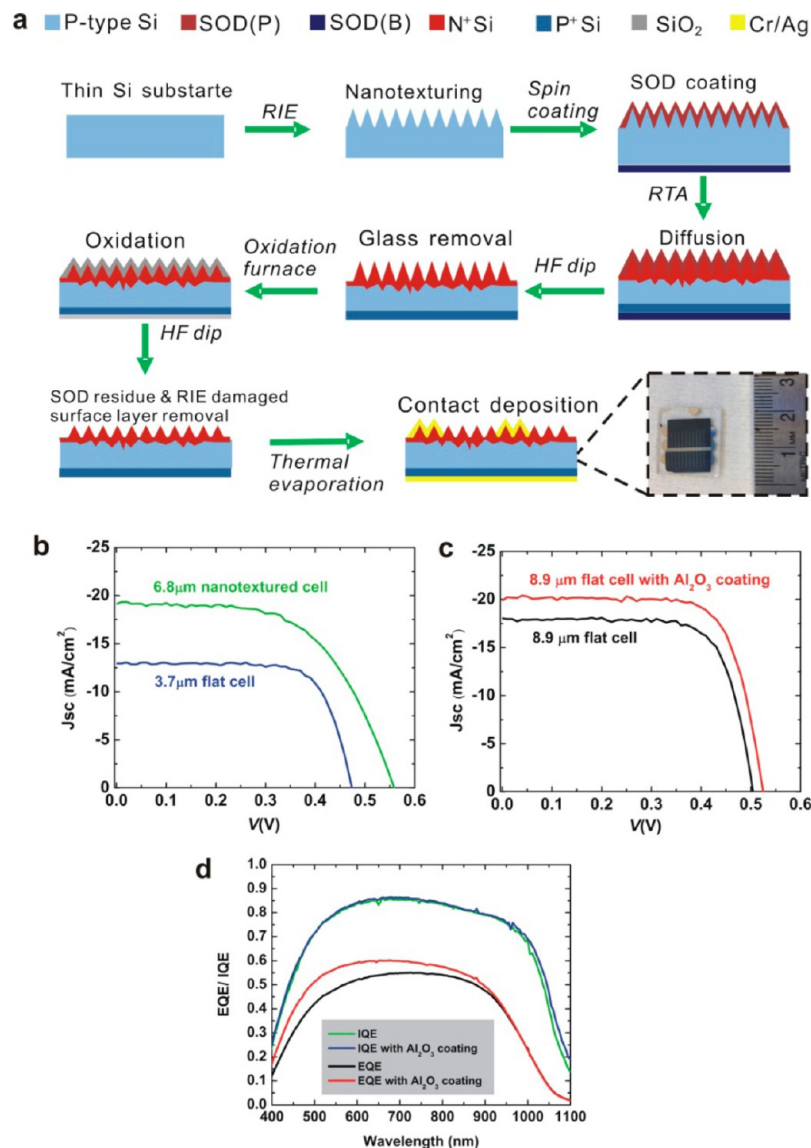
Figure 4. Schematic illustrations, optical image of the fabrication steps of free-standing ultrathin Si solar cells, and photovoltaic performance. (a) Schematic illustration of steps for fabricating free-standing ultrathin Si solar cells. The optical image shows a cell with dimensions of 1.5 cm × 1.2 cm. (b) I−V curves of a 6.8 μm thick front-side patterned cell and a 3.7 μm thick flat cell. (c) I−V curves of an 8.9 μm thick flat cell before and after 50 nm Al_2O_3 coating by ALD. (d) Comparison of EQE and IEQ curves before and after the Al_2O_3 coating.

seen that the front-side patterning has a good antireflection effect for a large absorption enhancement over a broadband wavelength range (see Figure 3e), and the back-side patterning further improves the absorption in the long wavelength range by efficient light trapping (see Figure 3f). Even though each patterning process removes some of the absorption materials, the surface textures still enhance the absorption by a large amount. The enhancements can be seen more clearly in Figure 3g, which shows the short circuit current density (J_{sc}) (assuming 100% internal quantum efficiency, calculated from light absorption) generated by the Si films with different texturing designs. There are large enhancements in the photocurrent by introducing the top-side antireflection surface texture for all of films with four different thicknesses, whereas the advantage of the back-side surface texture is more obvious for ultrathin film. For example the flat 3.0 μm thick sample generates a short circuit current of 10.6 mA/cm², which is increased to 19.4 mA/cm² by introducing the front-side

nanocone array texture, and further increased to 24.4 mA/cm² by adding the back-side nanodome array texture. For the ultrathin films, even with good antireflection, the light path inside the films is still too short to sufficiently absorb light over a large part of the whole spectrum, thus light scattering effect by the bottom-side texture becomes necessary for light trapping. This double-sided nanotexture design enables large light absorption enhancement with a 130% increase in J_{sc} for the 3.0 μm thick Si film. Remarkably, even for a 2.3 μm-thick film (see Figure 3b), it is still robust enough to be patterned on both sides without attached supports.

In addition to nanotexturing processing, we fabricated a PV device on the ultrathin Si films without supporting substrates and fully demonstrate their processability. Both flat and nanotextured cells were fabricated. Figure 4a schematically illustrates the fabrication steps. The process begins with the free-standing thin Si films etched from a p-type, boron-doped, single-crystalline, double-side polished wafer with a resistivity of

10−20 Ω·cm by KOH etching. The thin Si film is then patterned with nanocone array on one side with a periodicity of 450 nm and height of about 640 nm. The p−n junction and the back surface highly doped layer are made by rapid thermal diffusion (RTD) of impurities from spin-on sources. An oxide growth and HF removal step are introduced to help completely remove residue from the formed glass layer. The contacts were evaporated using a thermal evaporator. The optical image in Figure 4a shows such solar cells with dimensions of 1.5 cm × 1.2 cm. The device size thus far is limited by the rapid thermal diffusion step where we use a quartz tube furnace with an inner diameter of 2.2 cm and the shadow mask size for contact evaporation. Large area devices can be potentially fabricated by the processes we describe here. Figure 4b shows I−V curves of a 6.8 μm thick nanotextured solar cell and a 3.7 μm thick flat cell under AM 1.5 illumination. The 6.8 μm thick cell, which has front-side nanocone array, shows a short-circuit current density, J_{SC}, of 19.1 mA/cm², an open-circuit voltage, V_{OC}, of 0.559 V, a fill factor, FF, of 0.58, and an overall solar-power conversion efficiency, η, of 6.2%. The 3.7 μm thick flat cell has an efficiency of 4.5% with a lower J_{SC} of 12.9 mA/cm² due to insufficient light absorption. Besides the nanostructure design for light trapping, we also apply the antireflection coating method on the ultrathin Si cells by atomic layer deposition (ALD) of 50 nm of Al_2O_3 after the contact evaporation. Figure 4c illustrates I−V curves for the same cell of 8.9 μm thick before and after coating. There is a 17% increase of the total efficiency, from 6.6% to 7.7% (see Table 2). The external

Table 2. Photovoltaic Properties of the Ultrathin Si Solar Cells with and without Light Trapping

	substrate thickness (μm)	J_{SC} (mA/cm²)	V_{OC} (v)	FF (%)	η (%)
nanocone textured	6.8	19.1	0.559	58	6.2
planar	3.7	12.9	0.474	74	4.5
planar	8.9	18.0	0.504	73	6.6
Al_2O_3 coating	8.9	19.9	0.525	74	7.7

quantum efficiency is enhanced over a broad band after the coating, especially in the short wavelength region (as shown in Figure 4e). By examining the internal quantum efficiency, which shows a slight enhancement in the long wavelength region, it can be concluded that improvement of the total efficiency is mainly owing to the antireflection effect of the Al_2O_3 layer. The results here demonstrate the full set of fabrication on free-standing ultrathin Si films. It is exciting that these free-standing ultrathin Si films survive multiple steps of processing.

In conclusion, we have fabricated large-area ultrathin monocrystalline Si films in a free-standing form, which shows excellent flexibility and can be directly handled and cut by scissors. We studied the light trapping effect in the ultrathin Si films by a double-sided nanotexture design, showing a large improvement in light absorption. We have fabricated PV devices on the ultrathin Si films, down to 3.7 μm thick. By patterning double-sided nanotextures and fabricating PV devices on the free-standing ultrathin films, we have demonstrated that they are robust enough to be processed without supporting substrates, which open up the opportunity of both-sided processing and potentially reduce the processing cost. The simple fabrication processes reported here may create new possibilities for ultrathin monocrystalline Si devices,

particularly in applications in photovoltaics and flexible electronics.

Methods. *Fabricating Ultrathin Si Films.* The ultrathin Si films were etched from double-side polished p-type (100) Si wafers (4 in. diameter, 10−20 Ω·cm, 300−375 μm thickness, WRS Materials), which were immersed in KOH with a concentration of 50 wt % at 90 °C for different duration of time to obtain different thickness. The etching rate is about 80 μm/h. The transmittance color of wafer through white light is used to judge the thickness of wafers.

Patterning Double-Sided Nanotextures. First, 450 nm diameter and 1000 nm diameter SiO_2 nanoparticles were separately synthesized by a modified Stober process.[1] The 450 nm nanoparticles were deposited as a monolayer on a free-standing ultrathin Si film by Langmuir−Blodgett (LB) assembly method. Oxygen (O_2) and trifluoromethane (CHF_3) plasmas were used to reduce the SiO_2 nanoparticle diameter, followed by chlorine (Cl_2), O_2, and sulfur hexafluoride (SF_6) plasma to transfer the pattern into Si film with a cone-shape finishing. After the nanocone fabrication, the Si film was cleaned with 6:1 buffered oxide enchant (BOE) for 1 min to remove the SiO_2 nanoparticle deposit on the backside of the Si film and any residue of SiO_2 nanoparticles on the front side which might be left after etching. The film was then coated with the 1000 nm SiO_2 particles as a uniform monolayer on the back side using LB method. Again, O_2 and CHF_3 plasmas were used to reduce the SiO_2 nanoparticle diameter, and then, with a different combination of the flow rates, they were used to transfer the pattern into the Si film with a nanodome finishing. The Si film was cleaned with 6:1 BOE again to remove the residue 1000 nm SiO_2 particles.

Fabricating Solar Cells. The free-standing ultrathin Si film was taped onto a 500 μm thick Si wafer using Kepton tape. Phosphorus spin-on dopant (SOD) (P-8545, thickness range of 2045A-2450A, Honeywell ACCUSPIN) was deposited by spin-coating (4000 rpm, 1 min) in air, followed by hot plate baking at 150 °C for 1 min. The Si film was released, flipped over, and taped onto the other side of the thick Si wafer. Boron spin-on dopant (B40, thickness range of 5170A-5570A, Honeywell ACCUSPIN) was deposited and baked on the other side of the film by the same procedure. The Si film was exposed to rapid thermal annealing at 1050 °C for 30 s followed by a step of 900 °C for 10 min to drive in the dopant into Si, rapidly cooled to room temperature, immersed in 6:1 BOE for 90 s to remove the SOD on both sides of the film, and then thoroughly washed with DI water to complete the doping process. A 25 nm thick SiO_2 layer was grown on both sides of the Si film in an oxidation and annealing furnace and then etched by 6:1 BOE for 90 s. This step helps to remove the SOD residue completely, and in the case for nanotextured film, it helps to remove the damaged surface Si layer by the RIE etching. We used a continuous thin film of 8 nm Cr/200 nm Ag as a bottom electrode and a finger-grid of the same film as a top electrode. The width of each finger was 80 μm, and the spacing between fingers was 920 μm.

In electrical measurements of the cell performances, we used silver paste to connect the back contact of the cell with a metal pad of 8 nm Cr/100 nm Ag evaporated on a glass slide and used the metal pad and the bus line in the front contact as the output terminals to connect the measuring equipment.

■ ASSOCIATED CONTENT

ⓢ Supporting Information

Device fabrication process videos (mpg). This material is available free of charge via the Internet at http://pubs.acs.org.

■ AUTHOR INFORMATION

Corresponding Author

*E-mail address: yicui@stanford.edu.

Notes

The authors declare no competing financial interest.

■ ACKNOWLEDGMENTS

■ REFERENCES

(1) Soref, R. A. *Proc. IEEE* **1993**, *81* (12), 1687−1706.

(2) Sarti, D.; Einhaus, R. *Sol. Energy Mater. Sol. Cells* **2002**, *72* (1−4), 27−40.

(3) Henry, J.; Livingstone, J. *Adv. Mater.* **2001**, *13* (12−13), 1022−1026.

(4) Acciarri, M.; Binetti, S.; Bollani, M.; Comotti, A.; Fumagalli, L.; Pizzini, S.; von Kanel, H. *Sol. Energy Mater. Sol. Cells* **2005**, *87* (1−4), 11−24.

(5) Cui, Y.; Lieber, C. M. *Science* **2001**, *291* (5505), 851−853.

(6) Cui, Y.; Zhong, Z. H.; Wang, D. L.; Wang, W. U.; Lieber, C. M. *Nano Lett.* **2003**, *3* (2), 149−152.

(7) Fahad, H. M.; Smith, C. E.; Rojas, J. P.; Hussain, M. M. *Nano Lett.* **2011**, *11* (10), 4393−4399.

(8) Grom, G. F.; Lockwood, D. J.; McCaffrey, J. P.; Labbe, H. J.; Fauchet, P. M.; White, B.; Diener, J.; Kovalev, D.; Koch, F.; Tsybeskov, L. *Nature* **2000**, *407* (6802), 358−361.

(9) Kelzenberg, M. D.; Turner-Evans, D. B.; Putnam, M. C.; Boettcher, S. W.; Briggs, R. M.; Baek, J. Y.; Lewis, N. S.; Atwater, H. A. *Energy Environ. Sci.* **2011**, *4* (3), 866−871.

(10) Kim, D. H.; Ahn, J. H.; Choi, W. M.; Kim, H. S.; Kim, T. H.; Song, J. Z.; Huang, Y. G. Y.; Liu, Z. J.; Lu, C.; Rogers, J. A. *Science* **2008**, *320* (5875), 507−511.

(11) Yoon, J.; Baca, A. J.; Park, S. I.; Elvikis, P.; Geddes, J. B.; Li, L. F.; Kim, R. H.; Xiao, J. L.; Wang, S. D.; Kim, T. H.; Motala, M. J.; Ahn, B. Y.; Duoss, E. B.; Lewis, J. A.; Nuzzo, R. G.; Ferreira, P. M.; Huang, Y. G.; Rockett, A.; Rogers, J. A. *Nat. Mater.* **2008**, *7* (11), 907−915.

(12) Garnett, E. C.; Yang, P. D. *J. Am. Chem. Soc.* **2008**, *130* (29), 9224−9225.

(13) Lee, D.-Y.; Kim, H.; Li, H.-M.; Jang, A. R.; Lim, Y.-D.; Cha, S. N.; Park, Y. J.; Kang, D. J.; Yoo, W. J. *Nanotechnology* **2013**, *24* (17), 175402.

(14) Jane, A.; Dronov, R.; Hodges, A.; Voelcker, N. H. *Trends Biotechnol.* **2009**, *27* (4), 230−239.

(15) Mavrokefalos, A.; Han, S. E.; Yerci, S.; Branham, M. S.; Chen, G. *Nano Lett.* **2012**, *12* (6), 2792−2796.

(16) Bedell, S. W.; Shahrjerdi, D.; Hekmatshoar, B.; Fogel, K.; Lauro, P. A.; Ott, J. A.; Sosa, N.; Sadana, D. *IEEE J. Photovolt.* **2012**, *2* (2), 141−147.

(17) Shahrjerdi, D.; Bedell, S. W. *Nano Lett.* **2013**, *13* (1), 315−320.

(18) Xie, C.; Cui, Y. *Proc. Natl. Acad. Sci. U.S.A.* **2010**, *107* (10), 4489−4490.

(19) Xie, C.; Hanson, L.; Cui, Y.; Cui, B. X. *Proc. Natl. Acad. Sci. U.S.A.* **2011**, *108* (10), 3894−3899.

(20) Tian, B. Z.; Zheng, X. L.; Kempa, T. J.; Fang, Y.; Yu, N. F.; Yu, G. H.; Huang, J. L.; Lieber, C. M. *Nature* **2007**, *449* (7164), 885−U8.

(21) Boukai, A. I.; Bunimovich, Y.; Tahir-Kheli, J.; Yu, J. K.; Goddard, W. A.; Heath, J. R. *Nature* **2008**, *451* (7175), 168−171.

(22) Chan, C. K.; Peng, H. L.; Liu, G.; McIlwrath, K.; Zhang, X. F.; Huggins, R. A.; Cui, Y. *Nat. Nanotechnol.* **2008**, *3* (1), 31−35.

(23) Hui, W.; Chan, G.; Jang Wook, C.; Ill, R.; Yan, Y.; McDowell, M. T.; Seok Woo, L.; Jackson, A.; Yuan, Y.; Liangbing, H.; Yi, C. *Nat. Nanotechnol.* **2012**, *7* (5), 310−315.

(24) Blakers, A. W.; Armour, T. *Sol. Energy Mater. Sol. Cells* **2009**, *93* (8), 1440−1443.

(25) Sun, Y.; Choi, W. M.; Jiang, H.; Huang, Y. Y.; Rogers, J. A. *Nat. Nanotechnol.* **2006**, *1* (3), 201−207.

(26) Zhang, R. Y.; Shao, B.; Dong, J. R.; Zhang, J. C.; Yang, H. *J. Appl. Phys.* **2011**, *110* (11), 113105.

(27) Han, S. E.; Chen, G. *Nano Lett.* **2010**, *10* (11), 4692−4696.

(28) Gjessing, J.; Sudbo, A. S.; Marstein, E. S. *J. Appl. Phys.* **2011**, *110* (3), 033104.

(29) Wang, K. X.; Yu, Z.; Liu, V.; Cui, Y.; Fan, S. *Nano Lett.* **2012**, *12* (3), 1616−1619.

(30) Hsu, C. M.; Connor, S. T.; Tang, M. X.; Cui, Y. *Appl. Phys. Lett.* **2008**, *93* (13), 133109.